Deriving Extracellular Vesicle Size From Scatter Intensities Measured by Flow Cytometry

Leonie de Rond,[1,2,3] Frank A. W. Coumans,[1,2,3] Rienk Nieuwland,[2,3] Ton G. van Leeuwen,[1,3] and Edwin van der Pol[1,2,3,4]

[1]Amsterdam UMC, University of Amsterdam, Biomedical Engineering and Physics, Meibergdreef 9, Amsterdam, The Netherlands
[2]Amsterdam UMC, University of Amsterdam, Laboratory Experimental Clinical Chemistry, Meibergdreef 9, Amsterdam, The Netherlands
[3]Amsterdam UMC, University of Amsterdam, Vesicle Observation Center, Meibergdreef 9, Amsterdam, The Netherlands
[4]Corresponding author: *e.vanderpol@amc.uva.nl*

Flow cytometry is commonly used to investigate the potential for extracellular vesicles (EVs) to be biomarkers of disease. A typical flow cytometer detects fluorescence and scatter intensities of single EVs in arbitrary units. These arbitrary units complicate data interpretation and data comparison between different flow cytometers. For example, comparison of detected EV concentrations requires knowledge of the detectable EV sizes. Using Mie theory and knowledge of the optical configuration of the flow cytometer, EV size can be derived from the scatter intensity for a given EV refractive index. Here, a protocol is described to derive the size of EVs and other nanoparticles from the scatter intensity. The resulting size distribution allows the comparison of data between flow cytometers, which is a prerequisite for clinical application of EVs as biomarkers and may advance other fields where sizing of nanoparticles is essential.

Keywords: exosome • extracellular vesicles • flow cytometry • light scattering • microparticle

How to cite this article:
de Rond, L., Coumans, F. A., Nieuwland, R., van Leeuwen, T. G., & van der Pol, E. (2018). Deriving extracellular vesicle size from scatter intensities measured by flow cytometry. *Current Protocols in Cytometry*, e43. doi: 10.1002/cpcy.43

INTRODUCTION

To investigate the clinical potential of extracellular vesicles (EVs), the concentration of EV subtypes is commonly measured by flow cytometry (Gardiner et al., 2016). A typical flow cytometer detects forward-scattered light (FSC), side-scattered light (SSC), and fluorescence of single EVs. However, flow cytometers differ in sensitivity, and all intensities are presented in arbitrary units (Fig. 1A), impeding data interpretation and data comparison between flow cytometers (van der Pol, de Rond, et al., 2018; van der Pol, Sturk, et al., 2018).

Since light scattering depends on the particle size and refractive index, the measured scatter intensity contains information about the EV size. Throughout this article, size is defined as the diameter of the particle. By taking into account the optical configuration

Current Protocols in Cytometry e43
Published in Wiley Online Library (wileyonlinelibrary.com).
doi: 10.1002/cpcy.43

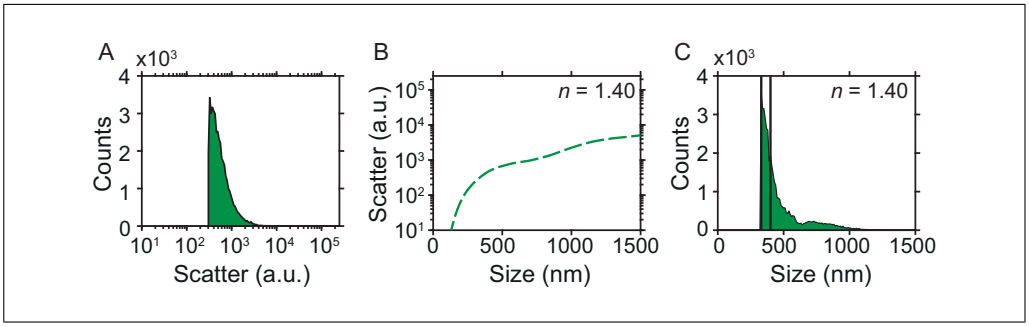

Figure 1 (**A**) Side scatter intensity histogram in arbitrary units (a.u.) of CD61-PE-positive platelet extracellular vesicles measured by flow cytometry (BD LSRFortessa). The trigger was set on side scatter with a threshold of 300 a.u., which corresponds to a scattering cross section of 207 nm^2. (**B**) Calibrated side scatter intensity versus size (diameter) for the LSRFortessa, as derived using Mie theory and assuming a refractive index (*n*) of 1.40 for the platelet extracellular vesicles (Gardiner et al., 2014; Kolesnikova et al., 2006; Konokhova et al., 2012). (**C**) Size distribution derived from the scatter intensities in (A) using the scatter-to-size relationship in (B). The vertical lines contain 47% of the counts and are positioned at 330 nm and 400 nm.

of the flow cytometer, Mie theory can be used to relate scatter intensities to EV size for a given EV refractive index (Fig. 1B; Bohren & Huffman, 1983). In other words, after calibration, Mie theory allows conversion of scatter intensities in arbitrary units (Fig. 1A) to the size of the detected EVs in nm (Fig. 1C; Fattaccioli et al., 2009; van der Pol et al., 2012).

The scatter intensity-to-size relationship has many applications. For EVs, the relationship can be used to compare EV concentrations within the same size range for different flow cytometers (van der Pol, Sturk, et al., 2018). This is particularly useful because flow cytometers differ in sensitivity, and the EV concentration decreases with increasing size. For example, an increase of the lower detection limit from 330-nm EVs to 400-nm EVs (Fig. 1C) would result in a 47% decrease of the detected platelet EV counts. Furthermore, a size distribution of EVs can be created to confirm the anticipated size range or to compare data to other techniques, such as electron microscopy (van der Pol, Coumans, & Grootemaat, et al., 2014). Since, unlike cells, the size of EVs can vary by more than an order of magnitude, knowledge of this EV size distribution is likely to be more important for the interpretation of results than it is for cells. Finally, scatter-based sizing is also applicable to nanoparticles other than EVs, such as bacteria, viruses, and nanomaterials (Foladori, Quaranta, & Ziglio, 2008; Koch, Robertson, & Button, 1996; Steen, 2004; van der Pol, Coumans, & Grootemaat, et al., 2014).

The objective of this article is to describe a protocol to derive the size of EVs and other nanoparticles from the scatter intensities measured by a flow cytometer.

BASIC PROTOCOL

FROM SCATTER INTENSITY TO EXTRACELLULAR VESICLE SIZE

The purpose of this protocol is to derive the size of EVs and other nanoparticles from the scatter intensities measured by a flow cytometer. In the first step, the scatter channel needs to be calibrated, which means that the arbitrary units of the scatter channel will be related to the size and refractive index of reference beads. The calibration step includes: (1) a measurement of scattering intensities of beads with a known size and refractive index; (2) a theoretical description of the relationship between the scattering intensity, size, and refractive index of the beads by Mie theory; and (3) a fitting procedure to relate the data to the theory. After calibration, Mie theory can be used to calculate the scatter-to-size relationship for particles with a different refractive index than the reference beads. The scatter-to-size relationship can in turn be used as a lookup table to determine the size

of EVs and other nanoparticles. Whereas the Basic Protocol requires programming, the three alternate protocols use compiled software to perform Mie calculations.

Materials

Monodisperse polystyrene beads of at least four different sizes
Distilled or deionized water, filtered using a ≤0.22-μm filter

Flow cytometer with the sensitivity to detect polystyrene beads <1 μm with the scatter channel that will be calibrated (hereinafter *the scatter channel*)
Numerical computing environment (e.g., LabVIEW, MATLAB, Python)

Protocol steps

1. Select settings of the flow cytometer optimal for nanoparticle detection (see Critical Parameters).
2. Run filtered water as a control for background counts.
3. Dilute polystyrene beads in filtered water to a concentration that is appropriate for the flow cytometer. Ensure you are measuring single beads by sonicating the beads prior to dilution and checking for swarm as described in van der Pol et al. (2012).

   Light scattering intensities of the different beads should approximately cover the dynamic range of the scatter channel. Preferably, the beads have a mean size determined with an uncertainty <3% and a coefficient of variation (CV) <10%.

   Select polystyrene beads that do not aggregate in distilled or deionized water, or add a surfactant to prevent aggregation before measurement.
4. Run polystyrene bead samples of different sizes separately. Measure ≥500 beads per sample.
5. For each bead sample, obtain the median of the scattering intensity of the bead population using the following procedure:

   a. Gate all events corresponding to the beads at the height-parameter of the scatter channel (Fig. 2A).
   b. Determine median and (robust) CV of the peak.

      The CV of the peak, defined as the standard deviation divided by the mean, is typically between 3% and 10%. The ratio of signal to background counts should preferably exceed 2. If background counts are present at the peak position, be sure to set a symmetrical gate around the bead peak.
6. For at least four bead sizes, plot the measured median scattering intensity versus the mean size of the beads (Fig. 2B).
7. Use Mie theory to calculate and plot which fraction of the illumination light is scattered towards the scatter detector by polystyrene beads (Fig. 2C).

   a. Obtain the refractive indices of water (Daimon & Masumura, 2007) and polystyrene (Kasarova, Sultanova, Ivanov, & Nikolov, 2007) at room temperature for the wavelength λ of the incident light in vacuum (see Table 1).
   b. Express the collection angles of the scatter detector in terms of the polar angle θ and the azimuthal angle ϕ using the spherical coordinate system of Figure 3.
      i. Obtain the numerical aperture NA of the lens which collects the light of the scatter detector.

         To obtain this information, please check the specification sheet of the flow cytometer or consult a service engineer. $NA = 1.2$ for the SSC detector of the BD FACSAria, FACSAria II, FACSCalibur, FACSCanto, FACSCanto II, FACSVerse, LSRFortessa, and LSR II and the Stratedigm S1000EX.

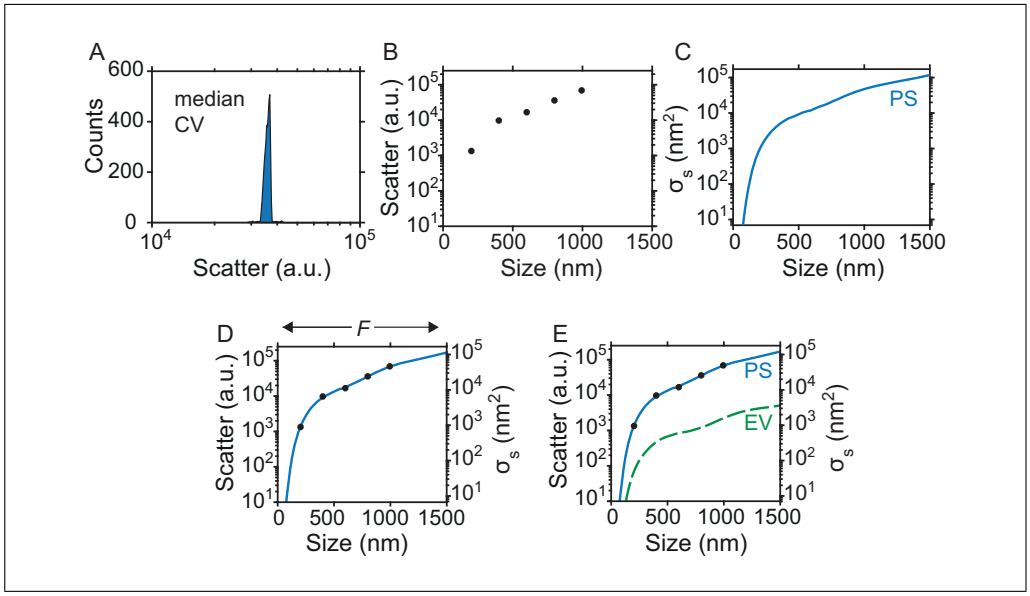

Figure 2 (**A**) Histogram of the side scatter intensity in arbitrary units (a.u.) of 800-nm polystyrene (PS) beads measured by flow cytometry (BD LSRFortessa). The histogram includes all events corresponding to the beads and is used to determine the median and CV of the peak (Basic Protocol steps 1 through 5). (**B**) Median of the side scatter intensity versus size (mean diameter) for five sizes of PS beads (Basic Protocol step 6). (**C**) Theoretical scattering cross section (σ_s) of PS beads for the side scatter channel of the flow cytometer versus size (Basic Protocol step 7). (**D**) Left axis: measured median of the side scatter intensity in a.u. versus size for five sizes of PS beads (symbols). Right axis: σ_s in nm^2 versus size (line). To relate the theory to the data, a scaling factor F is used to scale σ_s to the measured side scatter intensity (Basic Protocol step 8). In this example, $F = 1.45$ ($R^2 > 0.99$) results in a side scatter intensity that almost equals σ_s. (**E**) Similar to (D) but with the relationship for platelet extracellular vesicles (EV; assuming $n = 1.40$) added (Basic Protocol step 9).

Table 1 Refractive Indices of Water and Polystyrene at 20°C for Different Wavelengths of the Incident Light in Vacuum

Wavelength (nm)	Refractive index water[a]	Refractive index PBS[b]	Refractive index polystyrene[c]
405	1.343	1.345	1.633
488	1.337	1.339	1.605
514	1.336	1.338	1.601
532	1.335	1.337	1.599
633	1.332	1.334	1.587

[a]Daimon & Masumura, 2007.
[b]Kindt, 2012.
[c]Kasarova et al., 2007.
All refractive indices mentioned in the text are for a wavelength of 488 nm.
PBS, phosphate-buffered saline.

ii. Calculate the maximum propagation angle α of the lens relative to its optical axis:

$$\alpha = \sin^{-1}\left(\frac{NA}{n_m}\right)$$

Equation 1

where n_m is the refractive index of the medium.

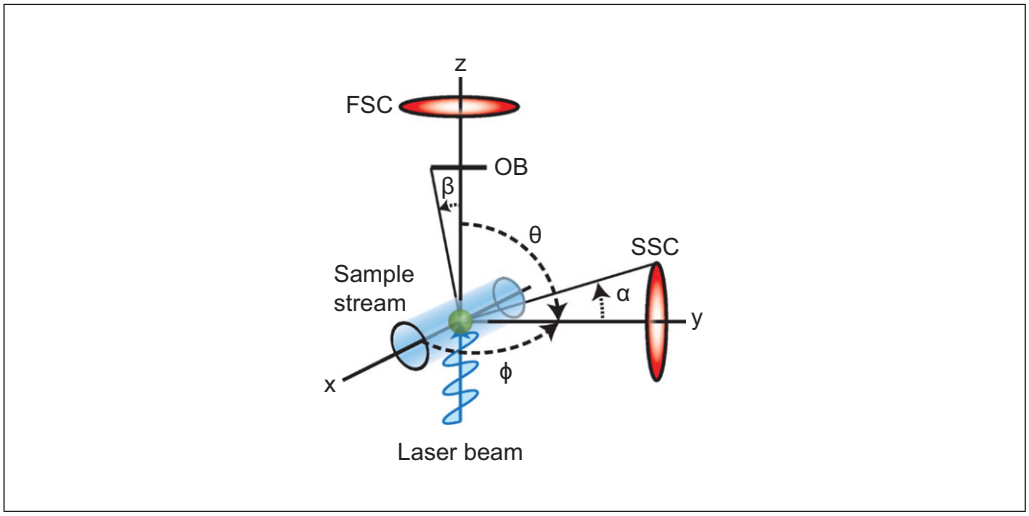

Figure 3 Spherical coordinate system used to calculate the fraction of the illumination light that is scattered towards the scatter detector in a flow cytometer. The electric field component of the laser beam is polarized in the *xz* plane and propagates through the cylindrical sample stream towards the particle (green sphere). For side scatter (SSC), the numerical aperture of the lens determines the acceptance angle α, which in turn determines the integration boundaries of the polar angle θ and the azimuthal angle ϕ in Equation 4. For forward scatter (FSC), the size of the obscuration bar (OB) determines angle β, which is the lower integration boundary of θ in Equation 4.

For calibration, n_m is the refractive index of water. For biological samples, n_m is usually the refractive index of phosphate-buffered saline (PBS; see Table 1). For a complete list of symbols and definitions as used in this article, see Table 2.

iii. For FSC with a spherical obscuration bar blocking all angles smaller than β, use β as the lower boundary $\theta_{\min}$, α as the upper boundary $\theta_{\max}$, 0° as the lower boundary $\phi_{\min}$, and 360° as the upper boundary $\phi_{\max}$. For SSC, use $\theta_{\min} = 90^\circ - \alpha$ and $\theta_{\max} = 90^\circ + \alpha$, and express $\phi_{\min}$ and $\phi_{\max}$ in terms of θ and α as follows:

$$\phi_{\min} = \sin^{-1}\left(\frac{\sin(90^\circ - \alpha)}{\sin(\theta)}\right)$$

Equation 2

$$\phi_{\max} = 180^\circ - \phi_{\min}$$

Equation 3

c. Use a numerical computing environment to solve Equation 4 to calculate the scattering cross section σ_s in nm^2, which describes the fraction of light that is scattered towards the scatter detector (see Background Information):

$$\sigma_s = \int_{\phi_{\min}}^{\phi_{\max}} \int_{\theta_{\min}}^{\theta_{\max}} \frac{|S_1|^2 \sin^2\phi + |S_2|^2 \cos^2\phi}{k^2} \sin\theta \, d\theta \, d\phi$$

Equation 4

where $\phi_{\min}$ and $\phi_{\max}$ are the integration boundaries of the azimuthal angle ϕ (Fig. 3); $\theta_{\min}$ and $\theta_{\max}$, the integration boundaries of the polar angle θ; S_1 and S_2, the amplitude scattering matrix elements; and $k = 2\pi n_m/\lambda$, the wavenumber. The parameters S_1 and S_2 depend on the particle diameter d and particle refractive index n_p, as well as n_m, k, and θ, and are thoroughly described in chapter 4 of Bohren & Huffman (1983). For n_p and n_m, take the refractive indices obtained

Table 2 Overview of Symbols and Their Definition as Used in the Manuscript

Symbol	Definition	Units
α	Maximum propagation angle of the detection lens	° or radians
β	Maximum angle blocked by the obscuration bar	° or radians
θ	Polar angle as specified in Figure 3	° or radians
λ	Wavelength of the incident light in vacuum	nm
σ_s	Scattering cross section	nm^2
ϕ	Azimuthal angle as specified in Figure 3	° or radians
d	Particle diameter	nm
F	Linear scaling factor relating measured scatter intensity to theoretical scattering cross section	a.u./nm^2
I	Median scattering intensity measured by the flow cytometer	a.u.
k	Wavenumber of the incident light in the medium	rad/nm
NA	Numerical aperture	
n_m	Medium refractive index	
n_p	Particle refractive index	
S_1, S_2	Amplitude scattering matrix elements in Mie theory	

a.u., arbitrary units.

in step 7a. For the integration boundaries, take the values obtained in step 7biii. Solve Equation 4 for multiple values of d within the dynamic range of the scatter channel (Fig. 2C).

For most programming languages, free scripts are available to calculate S_1 and S_2. Alternatively, compiled software is available to directly solve Equation 4 (see Alternate Protocols 1, 2, and 3).

8. Solve Equation 5 by linear regression to obtain the scaling factor F, which relates the measured median scattering intensity I of polystyrene beads in arbitrary units to their theoretical scattering cross section σ_s in nm^2 (Fig. 2D).

$$\log_{10}(I) = \log_{10}(F\sigma_s)$$

Equation 5

Both sides of Equation 5 are log-transformed to ensure equal contribution of high and low scatter intensities in determining the scaling factor.

9. Solve Equation 4 for the refractive index of EVs (e.g., $n_p = 1.40$ for platelet EVs; Gardiner et al., 2014; Kolesnikova et al., 2006; Konokhova et al., 2012) and multiple values of d within the dynamic range of the scatter channel. Multiply the calculated scattering cross sections by F to obtain the relationship between the measured scattering intensity of the particles of interest and their size (Fig. 2E):

$$I = F\sigma_s$$

Equation 6

10. Derive the size of EVs from their scatter intensities.

    a. Run the EV sample(s) at the same settings as the polystyrene bead samples.
    b. Relate the scatter intensities of EVs to their size by interpolating the scatter-to-size relationship from step 9 within the size range where the function is monotonic (i.e., the size range where a measured scatter intensity corresponds to only one particle size).

FROM SCATTER INTENSITY TO EXTRACELLULAR VESICLE SIZE WITH FREE MIE CALCULATION SOFTWARE

ALTERNATE PROTOCOL 1

Instead of writing your own scripts, free software can be used to solve Equation 4. Alternate Protocol 1 describes the derivation of EV size from the scatter intensity by using free software to perform the Mie calculations.

Additional Materials *(also see the Basic Protocol)*

Mie calculation software, such as MiePlot (Laven, 2018) or MieConScat (Rosenberg, 2018)

Protocol steps

1. Follow steps 1 to 7b as described in the Basic Protocol.
2. Use free software, such as MiePlot (Laven, 2018) or MieConScat (Rosenberg, 2018), to calculate the scattering cross section σ_s in nm^2. For n_p and n_m, take the refractive indices obtained in step 7a of the Basic Protocol. For the integration boundaries, take the values obtained in step 7biii of the Basic Protocol. Calculate the scattering cross section for multiple values of d within the dynamic range of the scatter channel.

   This approach may have limited ability to accurately specify the collection angles. For example, MiePlot does not allow specifying the integration boundaries of ϕ. Instead, MiePlot integrates ϕ from 0° to 360°. For SSC detectors, this limitation reduces the accuracy of the theoretical description.
3. Follow steps 8 to 10 as described in the Basic Protocol.

FREE SEMI-AUTOMATED DETERMINATION OF EXTRACELLULAR VESICLE SIZE FROM SCATTER INTENSITY

ALTERNATE PROTOCOL 2

FCM Scatter-Diameter Software (*http://www.joshuawelsh.co.uk*; Welsh, 2018) is available to automate steps 6 to 10 of the Basic Protocol. FCM Scatter-Diameter Software is limited to SSC detectors that are symmetrically placed at the y axis of Figure 3.

Additional Materials *(also see the Basic Protocol)*

FCM Scatter-Diameter Software (*http://www.joshuawelsh.co.uk*; Welsh, 2018)

Protocol steps

1. Follow steps 1 to 5 as described in the Basic Protocol.
2. Use FCM Scatter-Diameter Software to calculate and plot which fraction of the illumination light is scattered towards the scatter detector by polystyrene beads and EVs.

   a. Use the refractive index converter to obtain the refractive index of polystyrene at room temperature for λ.
   b. Enter the mean diameter, median scattering intensity, and refractive index of the polystyrene beads into the bead input table.
   c. Either let FCM Scatter-Diameter Software approximate α from the data provided in step 2b, or solve Equation 1 to calculate the maximum propagation angle α and add it to the modeling settings.

      Approximating α from the data provided in step 2b does not require knowledge of the NA of the lens and corrects for uncertainties in the NA of the lens.
   d. Run FCM Scatter-Diameter Software to solve Equation 4, and relate the measured median scattering intensity I of polystyrene beads and the particles of interest in arbitrary units to their theoretical scattering cross section σ_s in nm^2 (Fig. 2D).

3. Derive the size of EVs from their scatter intensities.

   a. Run the EV sample(s) at the same settings as the polystyrene beads samples.
   b. Relate the scatter intensities of EVs to their size by interpolating the scatter-to-size relationship from step 2d within the size range where the function is monotonic (i.e., the size range where a measured scatter intensity corresponds to only one particle size).

ALTERNATE PROTOCOL 3

AUTOMATED DETERMINATION OF EXTRACELLULAR VESICLE SIZE FROM SCATTER INTENSITY

Rosetta Calibration (Exometry) is a commercial kit that automates the Basic Protocol. Rosetta Calibration relates scatter to size for each scatter detector with the sensitivity to detect 400-nm polystyrene beads (van der Pol, Sturk, et al., 2018). In contrast to the Basic Protocol, Rosetta Calibration: (1) corrects for deviations of the actual alignment of a lens from the specified alignment of a lens, (2) takes into account the angle-dependent transmission efficiency of a lens, (3) takes into account rectangular obscuration bars, (4) corrects for refraction of light in jet in air systems (e.g., BD Influx, BC Astrios), and (5) describes the scatter-to-diameter relationship of flow cytometers with asymmetrically placed lenses (e.g., Apogee).

Additional Materials *(also see the Basic Protocol)*

Rosetta Calibration beads and software (Exometry)

Protocol steps

1. Follow steps 1 and 2 of the Basic Protocol.
2. Run the Rosetta Calibration beads as described by the manufacturer. Measure ≥500 events per bead peak.
3. Load the .fcs file of step 2 in Rosetta Calibration software, and select the scatter detector to calibrate. Then click "Calibrate" to solve Equations 1 to 5 and relate scatter to the size of polystyrene beads.
4. Select the refractive index of EVs (e.g., $n_p = 1.40$ for platelet EVs), and click "Calculate" to solve Equations 4 and 6 and relate scatter to the size of EVs.
5. Derive the size of EVs from their scatter intensities.

   a. Run the EV sample(s) at the same settings as the polystyrene beads samples.
   b. Click "Export size distributions" to relate the scatter intensities of EVs to their size.

   Rosetta Calibration software will automatically add the size of EVs to a new channel "Diameter (nm)" in the flow cytometry data files.

COMMENTARY

Background Information

Mie theory applied to light scattering of EVs in flow cytometry

Flow cytometers measure the amount of scattered light from single EVs in suspension. Light scattering underlies basic optical phenomena, such as transmission, reflection, refraction, and diffraction, and becomes apparent near the interface of two substances with different refractive indices.

Mie theory is a theoretical description of light scattering by spherical particles (Bohren & Huffman, 1983), such as EVs. Mie theory calculates the angular distribution of scattered light as a function of the EV size and refractive index, the refractive index of the medium, and the wavelength and polarization state of the laser beam. The scattered intensity [W], or more correctly the scattered power, measured at the detector (Fig. 1A) can be described as the product of the irradiance [$W \cdot m^{-2}$] of incident light and the scattering cross section (σ_s[m^2]). This scattering cross section is the effective area of collision between the incident light and

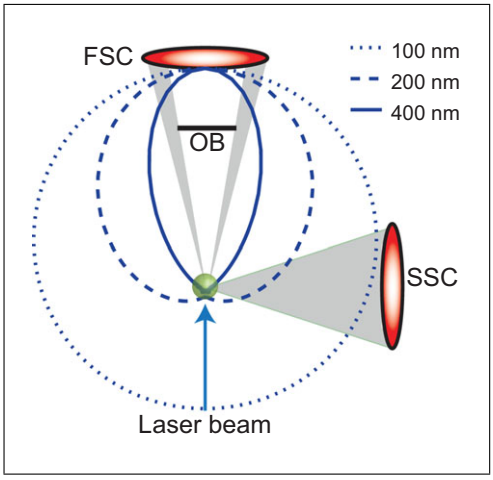

Figure 4 Normalized angular distribution of scattered light (i.e., phase function [dark blue]) of a 100-, 200-, and 400-nm polystyrene bead ($n = 1.605$) in water ($n = 1.33$). The collection angles on forward (FSC) and side scatter (SSC), together with the obscuration bar (OB), determine which fraction of the phase function contributes to the measured intensity. The electric field component of the laser beam (blue arrow) is perpendicular to the page.

a particle and relates the measured scattered intensities to particle size and refractive index. The scattering cross section can be computed from the angular distribution of scattered light if the collected scattering angles (θ, ϕ), wavelength (λ), and polarization state are known. Whereas the term scattering cross section commonly refers to integration of Equation 4 over 4π, in this article the term refers to integration of Equation 4 over the collection angles of the detector.

Assuming that the EV is in focus of the lens, the collected scattering angles are determined by the numerical aperture (*NA*) of the lens and the position of the lens with respect to the laser beam (Fig. 4). The wavelength and polarization can be retrieved from the specifications of the manufacturer. Furthermore, a scaling factor (F) is needed to account for the irradiance of the laser beam, transmission efficiency of the optics, quantum efficiency of the detector, and electronics processing. The scaling factor can be derived from calibration with particles of known scattering cross sections (i.e., beads of known size and refractive index), as described in step 8 of the Basic Protocol. Using the protocols presented here, the scatter intensities measured by a flow cytometer can be expressed as the size of the measured particle.

For EVs <1 μm, the size directly affects the angular distribution of scattered light (Fig. 4). For EVs of the same size, the amplitude of the scattered light increases with the refractive index contrast between the EV and the surrounding medium. All refractive indices are wavelength dependent. The refractive index of EVs was found to be between 1.37 and 1.45 (Gardiner et al., 2014; Konokhova et al., 2012; van der Pol, Coumans, Sturk, Nieuwland, & van Leeuwen, 2014), but may vary between individual EVs as it depends on its composition. The fact that these refractive indices are close to the refractive index of PBS ($n = 1.339$) explains the dim scatter intensities of EVs measured in flow cytometry.

Applications of Mie theory for nanoparticle sizing

The use of flow cytometric light scattering for sizing was first described by Tycko, Metz, Epstein, & Grinbaum (1985). Using Mie theory, the volume of red blood cells was determined, which correlated well ($r \geq 0.94$) with reference values determined using hematocrits and red blood cell counts. In the submicrometer regime, scatter-based sizing was first applied to small bacteria (Koch et al., 1996) and since then to viruses (Steen, 2004), bacteria in wastewater (Foladori et al., 2008), DNA containing nanoparticles (van Gaal, Spierenburg, Hennink, Crommelin, & Mastrobattista, 2010), platelet microparticles (Chandler, Yeung, & Tait, 2011), and EVs from colorectal cancer patients (Tian et al., 2018).

With at least two scatter detectors, the size and refractive index of EVs can be derived, making the assumption of a refractive index superfluous. Particle size and refractive index have been derived from FSC and SSC for a modified flow cytometer (Green, Sosik, Olson, & DuRand, 2003) and a commercial flow cytometer (van der Pol, de Rond, et al., 2018). In a more extreme example, size and refractive index have been derived using scanning flow cytometry, which measures scatter over a whole range of collection angles (Maltsev, 2000).

In comparison to other sizing methods, scatter-based sizing had a relative size accuracy $<5\%$ on reference beads, thereby outperforming dedicated sizing techniques such as resistive pulse sensing (RPS) and nanoparticle tracking analysis (NTA; van der Pol, Coumans, & Grootemaat, et al., 2014; van der Pol, Sturk, et al., 2018). EV sizing will probably be less accurate because the refractive index is not precisely known and may be different between EVs.

Alternative methods for sizing by flow cytometry

An alternative sizing method is based on the intensity of a fluorescent membrane dye. The fluorescence intensity is proportional to the surface area of the phospholipid membrane. Using liposomes of known size, a linear relationship between the fluorescence intensity of di-8-ANEPPS and size could be derived (Stoner et al., 2016). Similarly, EVs can be labeled with di-8-ANEPPS to enable fluorescence-based size estimation. Stoner and colleagues found good correlation between plasma EV size and concentration estimates using fluorescence sizing and NTA. However, the staining density of di-8-ANEPPS should be constant for applicability. Thus, either the amount of dye needs to be approximately matched to the number of EVs, or an excess of dye should be used so that the membrane becomes saturated with dye. Furthermore, di-8-ANEPPS also labels proteins, so the protein background needs to be negligible (de Rond et al., 2018). Another practical disadvantage is the commercial absence of labeled, monodisperse liposomes to relate fluorescence intensity to size.

Another frequently applied method to estimate the size of the measured EVs is by setting a size gate based on scatter intensities of reference particles of known size. This so-called "microparticle gate" is often set between beads of a known size, and all events that fall within that gate are regarded as EVs (Arraud, Gounou, Linares, & Brisson, 2015; Lacroix et al., 2010; Robert et al., 2009). However, the refractive index of these beads differs from that of EVs. Especially, the refractive index of polystyrene ($n = 1.605$ versus $n = 1.40$ for platelet EVs) causes the scatter intensity of a polystyrene bead to be a factor 6 to 40 higher than the scatter intensity of an EV of the same size (van der Pol, Sturk, et al., 2018). This approach thus leads to an underestimation of the size of the EVs. Silica beads ($n = 1.463$) have been proposed as an alternative (Chandler et al., 2011; Zhu et al., 2014), since they have a refractive index closer to the EV refractive index. The scatter intensity of a silica bead is, however, still a factor 2 to 5 higher than that of an EV of the same size, which is why the silica bead approach will also lead to an underestimation of the true EV size (van der Pol, Sturk, et al., 2018). Liposomes would be a better reference material, since they are also spherical vesicles with a phospholipid membrane, which makes their refractive index closer to that of EVs. However, due to the absence of proteins, the refractive index of liposomes is probably lower than that of EVs (Nolan, 2015). Moreover, monodisperse liposomes of multiple discrete sizes are difficult to obtain. Alternatively, hollow silica beads can be used as reference particles for EVs (Varga et al., 2018). Altogether, the direct use (i.e., without the use of Mie theory) of reference particle sizes to estimate EV size from light scatter requires a monodisperse (CV $< 10\%$) reference particle with the same refractive index as EVs.

Assumptions and applicability

System assumptions

Several assumptions underlie the Basic Protocol described here. With regard to the system, the three key assumptions for the Mie model described in the Basic Protocol are: accurate specification of collection angles, plane wave illumination, and particles passing through the focus of the lens. A mismatch between true and specified collection angles can lead to wrong theoretical descriptions of the data. Measuring the collection angles is possible but requires dismantling the flow cytometer and optical expertise. The plane wave assumption may not be applicable for flow cytometer designs with highly focused illumination beams, as sometimes found in flow cytometers dedicated to nanoparticle detection. For highly focused beams (spot size $\approx \lambda$; Lock & Gouesbet, 2009), the generalized Lorenz-Mie theory is needed, which requires exact specification of the illuminating focus. Furthermore, the model assumes that all particles are in focus in the axial and lateral direction. For the typical flow cytometer, the fluidics appear to be adequate to ensure the particle is in focus (van der Pol, Sturk, et al., 2018), but confocalization to suppress noise will result in a stricter position tolerance.

Particle assumptions and applicability

With regard to the particles, the two key assumptions are spherical particles and a known refractive index that is homogenously distributed within the particle. The spherical particle assumption is applicable to EVs, since 95% of EVs were found to be spherical (Arraud et al., 2014). The Mie model is, however, not appropriate for larger particles, such as platelets, because they are insufficiently spherical and contain an intracellular structure of sufficient dimensions to make a detectable contribution to the angular distribution of scattered light. With regard to particle refractive index, we assume a homogeneous

and constant refractive index for both calibration beads and EVs. For polystyrene beads, the homogeneous sphere model is adequate as beads are made out of a single material. The actual refractive index of polystyrene beads is unknown but is assumed to be equal to bulk polystyrene. EVs, however, consist of a phospholipid membrane with a refractive index that differs from the refractive index of the intravesicular content. A concentric model with a core and a shell of different refractive indices might therefore be more appropriate to model light scattering by EVs. However, for a 450-nm EV the scattering cross section of the 4-nm thick phospholipid membrane ($n = 1.46$) is 10% of the scattering cross section of the core ($n = 1.37$). For EVs larger than 450 nm, a model comprising a uniform sphere with just the core refractive index can thus be considered adequate. Advanced programs allow use of either the homogeneous or concentric model, thereby expanding applicability of scatter-based sizing to particles with a homogeneous and concentric refractive index distribution.

The range of estimates for EV refractive index is 1.37 to 1.45 (Gardiner et al., 2014; Konokhova et al., 2012; van der Pol, Coumans, Sturk, et al., 2014). This range of refractive indices is so large that the wavelength dependency can be considered negligible for typical illumination wavelengths used by flow cytometers. In addition, for a given side scatter intensity on the BD LSRFortessa, an assumed homogeneous refractive index of 1.37 results in an EV size of 1110 nm, whereas an assumed refractive index of 1.45 results in an EV size of 275 nm. This example illustrates that the refractive index of EVs as well as the calibration beads should be carefully chosen. Furthermore, the overall size of agglomerated particles cannot be described by Mie theory because the enclosed medium will lead to a variable refractive index.

In these protocols, polystyrene beads are used as calibration particles. It is, however, possible to use any type of spherical particle for calibration, as long as the size and refractive index are known. In our hands, the refractive index of silica beads was found to be batch dependent, while we never encountered this problem with polystyrene beads.

As mentioned in step 10 of the Basic Protocol, scatter-based sizing can be applied for particle sizes within the monotonic part of the scatter-to-size relationship. When the relationship is not monotonic, a measured scatter intensity can correspond to more than one particle size. The threshold size from which the relationship is not monotonically increasing differs per flow cytometer. For most flow cytometers the threshold size is ≥ 1 μm; however, for some nonstandard flow cytometers (e.g., A50-micro, BD Influx), we have found this threshold size to be between 400 nm and 1 μm.

Critical Parameters

Because the EV size is determined from scatter intensities, increased sensitivity for scatter intensities directly translates into an increased accuracy of the determined size. The choice of scatter detector and instrument settings are therefore critical.

Generally, because of the small size and low refractive index of EVs, the most sensitive scatter channel should be used for EV sizing. If both scatter channels are sufficiently sensitive, the FSC channel will have a steeper scatter-to-size relationship for EVs <1 μm and thus higher resolution for sizing (van der Pol et al., 2012). Only scatter intensity with a negligible contribution of noise can be used for sizing. The noise level can be determined by using a pulsed laser to trigger on a fluorescence channel; the intensity measured in the scatter channel is then only noise. Alternatively, for a robust estimation of the noise, the filtered water measurement of Basic Protocol step 2 can be used. Scatter intensities higher than the median level of the noise + three times the standard deviation of the noise can be used for sizing, since these scatter intensities have a negligible contribution of noise. For triggering, scatter and/or fluorescence channels can be used. The trigger threshold is best set at a value that results in a low number of events in filtered water.

As mentioned before, a higher sensitivity results in a higher accuracy of the determined size. A low flow rate is therefore preferred over a high flow rate, since low flow rates give lower CVs. The CV is also influenced by the photomultiplier tube (PMT) voltage, which should be optimized for nanoparticles. Overall, any changes in the optical configuration or acquisition system should be followed by a new calibration of the scatter-to-size relationship.

Troubleshooting

Ideally, four or more polystyrene beads should be measured to ensure accurate determination of the scaling factor. If this is not possible, select other bead sizes or refractive indices to ensure detection of at least four different bead sizes.

Table 3 Anticipated Time Per Step for Routine Operation of the Basic Protocol

Protocol step	Anticipated time (min)
1. Flow cytometer settings	1
2. Run purified, distilled water	2
3. Dilute polystyrene beads	5
4. Run polystyrene beads	8
5. Obtain median scattering intensity	20
6. Plot median scatter intensity versus bead size	5
7. Calculate fraction of illumination light that is scattered to the detector	15
8. Obtain scaling factor F	5
9. Solve Equation 4 for n of the particles that require sizing	1
10. Interpolate the scatter-to-size relationship	2
Total time	**64**

A mismatch in slope between the model and the different bead peaks may be indicative of an inaccuracy in the optics specification. Note that some flow cytometer designs do not have a fixed distance between collection lens and flow cell, and a deviation from the specified *NA* may be probable for such systems. Furthermore, an offset between optical axis and either particle or detector may need to be accounted for in Equation 4.

High CVs (>10%) on the bead measurements may be indicative of particles not passing consistently through the focus of the lens or instability of the laser beam. A systematic deviation from focus may be accounted for in Equation 4, but high positional uncertainty will reduce model accuracy.

Troubleshooting the EV assumptions requires a procedure that isolates monodisperse EVs. Such a procedure is hitherto unavailable.

Anticipated Results

In step 5 of the Basic Protocol, the median and CV of the scattering intensity is to be determined for each of the polystyrene beads. Ideally the median and robust CV are used to minimize the influence of outliers (Shapiro and Leif, 2003). Furthermore, it is possible to quantify the accuracy of the scatter-versus-size relationship by calculating the coefficient of determination (R^2) of the relationship derived in Basic Protocol step 8 with the data of the polystyrene beads in Basic Protocol step 6.

Time Considerations

Table 3 shows the anticipated time per step for routine operation of the Basic Protocol. We assumed that flow cytometer settings optimal for nanoparticle detection have been previously established and that the required specifications and software are available (i.e., this is not the first time you perform the procedure). With automation and dilution from a bead stock, the total procedure can be reduced to 10 min.

Acknowledgements

We thank Dr. Joshua A. Welsh from the National Cancer Institute, Bethesda, Maryland for providing us with details about his FCM Scatter-Diameter Software. We acknowledge funding from the Netherlands Organisation for Scientific Research–Domain Applied and Engineering Sciences (NWO-TTW), research programs Perspectief CANCER-ID 14195 (LdR), VENI 13681 (FC), and VENI 15924 (EvdP).

Literature Cited

Arraud, N., Gounou, C., Linares, R., & Brisson, A. R. (2015). A simple flow cytometry method improves the detection of phosphatidylserine-exposing extracellular vesicles. *Journal of Thrombosis and Haemostasis*, *13*, 237–247. doi: 10.1111/jth.12767.

Arraud, N., Linares, R., Tan, S., Gounou, C., Pasquet, J.-M., Mornet, S., & Brisson, A. R. (2014). Extracellular vesicles from blood plasma: Determination of their morphology, size, phenotype and concentration. *Journal of Thrombosis and Haemostasis*, *12*, 614–627. doi: 10.1111/jth.12554.

Bohren, C. F., & Huffman, D. R. (1983). *Absorption and scattering of light by small particles*. New York: Wiley.

Chandler, W. L., Yeung, W., & Tait, J. F. (2011). A new microparticle size calibration standard for use in measuring smaller microparticles using a new flow cytometer. *Journal of Thrombosis and Haemostasis*, *9*, 1216–1224. doi: 10.1111/j.1538-7836.2011.04283.x.

Daimon, M., & Masumura, A. (2007). Measurement of the refractive index of distilled water from the near-infrared region to the ultraviolet region. *Applied Optics*, *46*, 3811. doi: 10.1364/AO.46.003811.

de Rond, L., van der Pol, E., Hau, C. M., Varga, Z., Sturk, A., van Leeuwen, T. G., & Nieuwland, R. (2018). Comparison of generic fluorescent markers for detection of extracellular vesicles by flow cytometry. *Clinical Chemistry*, *64*, 680–689. doi: 10.1373/clinchem.2017.278978.

Fattaccioli, J., Baudry, J., Émerard, J. D., Bertr, E., Goubault, C., Henry, N., & Bibette, J. (2009). Size and fluorescence measurements of individual droplets by flow cytometry. *Soft Matter*, *5*, 2232–2238. doi: 10.1039/b814954b.

Foladori, P., Quaranta, A., & Ziglio, G. (2008). Use of silica microspheres having refractive index similar to bacteria for conversion of flow cytometric forward light scatter into biovolume. *Water Research*, *42*, 3757–3766. doi: 10.1016/j.watres.2008.06.026.

Gardiner, C., Shaw, M., Hole, P., Smith, J., Tannetta, D., Redman, C. W., & Sargent, I. L. (2014). Measurement of refractive index by nanoparticle tracking analysis reveals heterogeneity in extracellular vesicles. *Journal of Extracellular Vesicles*, *3*, 25361. doi: 10.3402/jev.v3.25361.

Gardiner, C., Di Vizio, D., Sahoo, S., Théry, C., Witwer, K. W., Wauben, M., & Hill, A. F. (2016). Techniques used for the isolation and characterization of extracellular vesicles: Results of a worldwide survey. *Journal of Extracellular Vesicles*, *1*, 1–6. doi: 10.3402/jev.v5.32945.

Green, R. E., Sosik, H. M., Olson, R. J., & DuRand, M. D. (2003). Flow cytometric determination of size and complex refractive index for marine particles: Comparison with independent and bulk estimates. *Applied Optics*, *42*, 526–541. doi: 10.1364/AO.42.000526.

Kasarova, S. N., Sultanova, N. G., Ivanov, C. D., & Nikolov, I. D. (2007). Analysis of the dispersion of optical plastic materials. *Optical Materials*, *29*, 1481–1490. doi: 10.1016/j.optmat.2006.07.010.

Kindt, J. D. (2012). Optofluidic intracavity spectroscopy for spatially, temperature, and wavelength dependent refractometry. M.S. thesis. Fort Collins, CO: Colorado State University.

Koch, L. A., Robertson, B. R., & Button, D. K. (1996). Deduction of the cell volume and mass from forward scatter intensity of bacteria analyzed by flow cytometry. *Journal of Microbiological Methods*, *27*, 49–61. doi: 10.1016/0167-7012(96)00928-1.

Kolesnikova, I. V., Potapov, S. V., Yurkin, M. A., Hoekstra, A. G., Maltsev, V. P., & Semyanov, K. A. (2006). Determination of volume, shape and refractive index of individual blood platelets. *Journal of Quantitative Spectroscopy & Radiative Transfer*, *102*, 37–45. doi: 10.1016/j.jqsrt.2006.02.050.

Konokhova, A. I., Yurkin, M. A., Moskalensky, A. E., Chernyshev, A. V., Tsvetovskaya, G. A., Chikova, E. D., & Maltsev, V. P. (2012). Light-scattering flow cytometry for identification and characterization of blood microparticles. *Journal of Biomedical Optics*, *17*, 57006–57008. doi: 10.1117/1.JBO.17.5.057006.

Lacroix, R., Robert, S., Poncelet, P., Kasthuri, R. S., Key, N. S., & Dignat-George, F. (2010). Standardization of platelet-derived microparticle enumeration by flow cytometry with calibrated beads: Results of the International Society on Thrombosis and Haemostasis SSC Collaborative workshop. *Journal of Thrombosis and Haemostasis*, *8*, 2571–2574. doi: 10.1111/j.1538-7836.2010.04047.x.

Laven, P. (2018). *MiePlot*. Retrieved from *http://www.philiplaven.com/mieplot.htm*.

Lock, J. A., & Gouesbet, G. (2009). Generalized Lorenz-Mie theory and applications. *Journal of Quantitative Spectroscopy & Radiative Transfer*, *110*, 800–807. doi: 10.1016/j.jqsrt.2008.11.013.

Maltsev, V. P. (2000). Scanning flow cytometry for individual particle analysis. *Review of Scientific Instruments*, *71*, 243. doi: 10.1063/1.1150190.

Nolan, J. P. (2015). Flow cytometry of extracellular vesicles: Potential, pitfalls, and prospects. *Current Protocols in Cytometry*, *73*, 13.14.1–13.14.16. doi: 10.1002/0471142956.cy1314s73.

Robert, S., Poncelet, P., Lacroix, R., Arnaud, L., Giraudo, L., Hauchard, A., ... Dignat-George, F. (2009). Standardization of platelet-derived microparticle counting using calibrated beads and a Cytomics FC500 routine flow cytometer: A first step towards multicenter studies? *Journal of Thrombosis and Haemostasis*, *7*, 190–197. doi: 10.1111/j.1538-7836.2008.03200.x.

Rosenberg, P. (2018). *MieConScat*. Retrieved from *https://sourceforge.net/projects/mieconscat/*.

Shapiro, H. M., & Leif, R. C. (2003). Data analysis. In H. M. Shapiro (Ed.), *Practical flow cytometry*, 4th ed (pp. 225–256). Hoboken, New Jersey: John Wiley & Sons, Inc.

Steen, H. B. (2004). Flow cytometer for measurement of the light scattering of viral and other submicroscopic particles. *Cytometry. Part A*, *57*, 94–99. doi: 10.1002/cyto.a.10115.

Stoner, S. A., Duggan, E., Condello, D., Guerrero, A., Turk, J. R., Narayanan, P. K., & Nolan, J. P. (2016). High sensitivity flow cytometry of membrane vesicles. *Cytometry. Part A*, *89*, 196–206. doi: 10.1002/cyto.a.22787.

Tian, Y., Ma, L., Gong, M., Su, G., Zhu, S., Zhang, W., ... Yan, X. (2018). Protein profiling and sizing of extracellular vesicles from

colorectal cancer patients via flow cytometry. *ACS Nano*, *12*, 671–680. doi: 10.1021/acsnano.7b07782.

Tycko, D. H., Metz, M. H., Epstein, E. A., & Grinbaum, A. (1985). Flow-cytometric light scattering measurement of red blood cell volume and hemoglobin concentration. *Applied Optics*, *24*, 1355–1365. doi: 10.1364/AO.24.001355.

van der Pol, E., Coumans, F. A. W., Grootemaat, A. E., Gardiner, C., Sargent, I. L., Harrison, P., ... Nieuwland, R. (2014). Particle size distribution of exosomes and microvesicles determined by transmission electron microscopy, flow cytometry, nanoparticle tracking analysis, and resistive pulse sensing. *Journal of Thrombosis and Haemostasis*, *12*, 1182–1192. doi: 10.1111/jth.12602.

van der Pol, E., Coumans, F. A. W., Sturk, A., Nieuwland, R., & van Leeuwen, T. G. (2014). Refractive index determination of nanoparticles in suspension using nanoparticle tracking analysis. *Nano Letters*, *14*, 6195–6201. doi: 10.1021/nl503371p.

van der Pol, E., de Rond, L., Coumans, F. A. W., Gool, E. L., Böing, A. N., Sturk, A., ... van Leeuwen, T. G. (2018). Absolute sizing and label-free identification of extracellular vesicles by flow cytometry. *Nanomedicine: Nanotechnology, Biology, and Medicine*, *14*, 801–810. doi: 10.1016/j.nano.2017.12.012.

van der Pol, E., Sturk, A., van Leeuwen, T. G., Nieuwland, R., Coumans, F. A. W., & ISTH-SSC-VB Working Group (2018). Standardization of extracellular vesicle measurements by flow cytometry through vesicle diameter approximation. *Journal of Thrombosis and Haemostasis*, *16*, 1236–1245. doi: 10.1111/jth.14009.

van der Pol, E., Van Gemert, M. J. C., Sturk, A., Nieuwland, R., Van Leeuwen, T. G., Nieuwl, R., & Van Leeuwen, T. G. (2012). Single vs. swarm detection of microparticles and exosomes by flow cytometry. *Journal of Thrombosis and Haemostasis*, *10*, 919–930. doi: 10.1111/j.1538-7836.2012.04683.x.

van Gaal, E. V. B., Spierenburg, G., Hennink, W. E., Crommelin, D. J. A., & Mastrobattista, E. (2010). Flow cytometry for rapid size determination and sorting of nucleic acid containing nanoparticles in biological fluids. *Journal of Controlled Release*, *141*, 328–338. doi: 10.1016/j.jconrel.2009.09.009.

Varga, Z., van der Pol, E., Pálmai, M., Garcia-Diez, R., Gollwitzer, C., Krumrey, M., ... Nieuwland, R. (2018). Hollow organosilica beads as reference particles for optical detection of extracellular vesicles. *Journal of Thrombosis and Haemostasis*, Epub ahead of print. doi: 10.1111/jth.14193.

Welsh, J. A. (2018). *FCM Scatter-Diameter Software*. Retrieved from *http://www.joshuawelsh.co.uk/scatter-diameter-software/*.

Zhu, S., Ma, L., Wang, S., Chen, C., Zhang, W., Yang, L., ... Yan, X. (2014). Light-scattering detection below the level of single fluorescent molecules for high-resolution characterization of functional nanoparticles. *ACS Nano*, *8*, 10998–11006. doi: 10.1021/nn505162u.